SOLID FREEFORM FABRICATION OF TRANSPARENT FUSED QUARTZ USING A FILAMENT FED PROCESS

J. Luo[1], L. J. Gilbert[1], C. Qu[1], B. Morrow[1], D. A. Bristow[1], R. G. Landers[1], J. Goldstein[2], A. Urbas[2], E. C. Kinzel[1]*

1. Mechanical and Aerospace Engineering, Missouri University of Science and Technology 400 W. 13th St., Rolla, MO 65401

2. Air Force Research Laboratory, Materials and Manufacturing Directorate, Wright-Patterson Air-Force Base, OH, 45433

Abstract

Glass is a critical material for many scientific and engineering applications including optics, communications, electronics, and hermetic seals. Despite this technological relevance, there has been minimal research toward Additive Manufacturing (AM) of glass, particularly optically transparent glass. Additive Manufacturing of transparent glass offers potential advantages for lower processing costs for small production volumes, increased design freedom, and the ability to locally vary the optical properties of the part. Compared to common soda lime glass, fused quartz is better for AM since it has lower thermal expansion and higher index homogeneity. This paper presents a study of additive manufacturing of transparent fused quartz by a filament fed process. A CW CO_2 laser (10.6 μm) is used to melt glass filaments layer by layer. The laser couples to phononic modes in the glass and is well absorbed. The beam and melt pool are stationary while the work piece is scanned using a standard lab motion system. Representative parts are built to explore the effects of variable laser power on the properties of printed fused quartz. During printing the incandescent emission from the melt pool is measured using a spectrometer. This permits process monitoring and identifies potential chemical changes in the glass during printing. After deposition, the printed parts are polished and the transmission measured to calculate the absorption/scattering coefficient. Finally, a low-order thermal analysis is presented and correlated to experimental results, including an energy balance and finite volume analysis using Fluent. These results suggest that optical quality fused quartz parts with low absorption and high index of refraction uniformity may be printed using the filament-fed process.

Introduction

Additive Manufacturing (AM) is an increasingly popular technology used to create three dimensional parts using deposition processes. AM has long been used for creating structural elements where the transparency of the part was not among the important design constraints. Recently several groups have demonstrated using AM of optical components. This work has been primarily based on polymers and includes studies using ink-jet printing [1-3], ink jet printing with in-situ UV curing [4], The Selective Laser Sintering (SLS) of polymers infiltrated with indexed matched plastic in post processing [5], and multiphoton stereolithography (SLA) [6]. These process have allowed the rapid prototyping of non-imaging optics, display surfaces of arbitrary geometries, sensors, interactive devices [1-3, 7], and GRadient INdex (GRIN) devices.

The latter were created using layer-to-layer fabrication with locally adjusted indices of refraction [4].

While significant progress has been made in printing transparent polymers, polymers are typically used for low cost and low power optics. Inorganic materials like glasses are more suited to high-quality, high power optics because they have high transmissivity (particularly in the ultraviolet and infrared), glasses have lower coefficients of thermal expansion and, unlike polymers, their indices of refraction are thermally stable [8]. Like plastics, glass is amorphous and does not present crystalline boundaries for scattering. The SLS process has been used to print fused quartz [9], borosilicate [10], and soda-lime glasses [11, 12]. Extrusion techniques have been used to print bone scaffolds of bioactive glass [13], and to print pattern colored glass [14]. Marchelli et al. have demonstrated printing glass using an inkjet method with a maltodextrin binder that was burnt out in post processing [15]. These studies have focused on the ability to create dimensionally accurate glass parts, but rely on an organic binder that must be burnt-out in post processing. This leads to small gas inclusions which act as scattering sites and leave the final parts not transparent. Luo et al. previously showed that a continuous filament fed process was capable of printing fully dense and optically transparent soda lime glass [12]. This process is similar to the AM Fused Deposition Modeling (FDM) process for depositing thermoplastics and laser wire-deposition processes used in metal AM [16].s

Soda-lime glass includes additives to reduce its melting point and improve its workability. On the other hand, fused quartz is nearly pure silica. Fused quartz has a high thermal shock resistance due to its low coefficient of thermal expansion, and is more transmissive than soda-lime glass for ultraviolet and infrared (IR) wavelengths. A softening temperature in excess of 1600°C makes manufacturing fused quartz more challenging than soda-lime glass [17]. AM methods demonstrated for printing fused quartz do not produce transparent parts due to trapped bubbles [9]. This paper presents the study of an AM process that prints clear fused quartz, and explores the effects that laser power has on the morphologic and optical properties of the printed material. The optical quality of 2D walls is determined through transmittance, Modulation Transfer Function (MTF), and the calculation of the refractive index. Finally a thermal analysis is conducted to estimate the melt pool temperature for different laser powers with constant feed rates and scan speeds.

Experimental Procedure

The properties of fused quartz make it difficult to print transparent parts using conventional AM techniques. Nozzle based extrusion processes cannot be used due to the high transition temperature of quartz and the wetting of metal oxides which cause potential clogging issues. Due to its nonconductivity electric arc generated plasmas are also ineligible as an AM technique for quartz. However, by using a laser to heat a rigid filament external to the feeder, fused quartz can be continuously deposited onto a moving platform. An example of the experimental setup is illustrated in Figure 1.

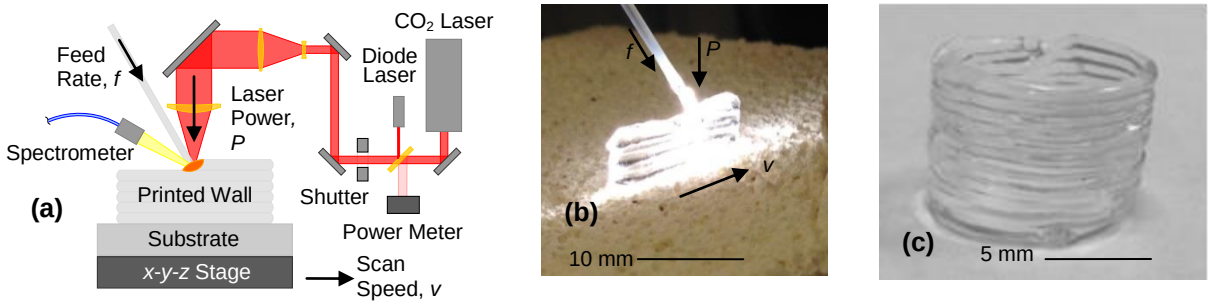

Fig. 1. Illustration and photograph of filament-fed fused quartz AM process

A ceramic refractory block is secured to numerically controlled 3 axis stages. This provides a material for the fused quartz to wet and thermally isolates the stages. The *x* and *y* stages (Thorlabs DDMS100) are actuated via direct-drive brushless servo motors. The build platform is raised and lowered by a scissor type lab-jack (Thorlabs L490MZ). Since fused quartz is opaque in the long-wave infrared portion of the electromagnetic spectrum [18], a fixed CO_2 laser beam (Synrad Evolution 125, $\lambda_0 = 10.6$ μm) is used as the energy source to maintain the melt pool.

Fused quartz has a low coefficient of thermal expansion (5×10^{-7} K^{-1}) [17], which is less than 10% of soda-lime glass. Cracking during the deposition and cooling process did not occur for small pieces of printed fused quartz (this does occur for similar soda-lime glass pieces [12]). For larger pieces a preheated substrate may be beneficial as thermal stresses may build up do to the increased thermal resistance of the pieces. For these experiments 1 mm diameter GE 214 fused quartz filaments are used as feedstock. The filaments are fed into the melt pool at a 45° angle from the normal using a custom designed wire feeder. This feeder was designed to be consistent with the literature on wire-fed metal AM [19-20] and is driven by a computer controlled stepper motor. The filament is manually aligned so that it passes through the intersection of the laser beam and the refractory block (or previous layer). The Full Width Half Maximum (FWHM) diameter of the laser beam is measured to be 200 μm at this intersection. During the experiment, 1% of the laser beam is reflected into a thermopile power meter (Ophir 10A –V1). The power delivered to the filament/workpiece can be determined in-situ by scaling this measurement. In order to ensure the stability of the laser, the laser was set to a constant power (measured variation ±1.5%) and is regulated with a water cooled shutter during processing. An OceanOptics USB-4000 fiber-coupled spectrometer is focused on the filament/workpiece intersection (mounted at a distance of 5 cm). The interrogation area the spectrometer is approximately a 3 mm diameter circle. This permits visible/NIR radiation emitted from the melt pool to be resolved spectrally.

For the following experiments, the fused quartz is deposited by a constant feeding of the filament into the melt pool. This process creates a single glass line with a uniform height and width. 3D structures are created by repeating this process after lowering the stage by a set amount.

Results and Discussion

Morphology result

The morphology of deposited fused quartz depends on the laser power, material feed rate and part scan speed. These process parameters, determine the temperature of the molten region. The temperature increases when the laser power increases, or the material feed rate or the part scan speed decreases. If the temperature of the molten region is too low, the filament is not sufficiently melted resulting in a failed part. If the temperature is too high, the melted glass starts to ball up at the end of the fiber due to the low viscosity. This causes the top layer to disconnect from previous layers resulting in a failed discontinuous part. For a material feed rate of 1 mm/s, a part scan speed of 0.5 mm/s, and laser powers of 30-50 W good fused quartz walls Fig. 2 (b) are produced: walls that are continuous and whose sides are normal to the build plane. Laser powers below 30 W and above 50 W results in failed walls. An example of a good wall, and both failure conditions are shown in Fig. 2.

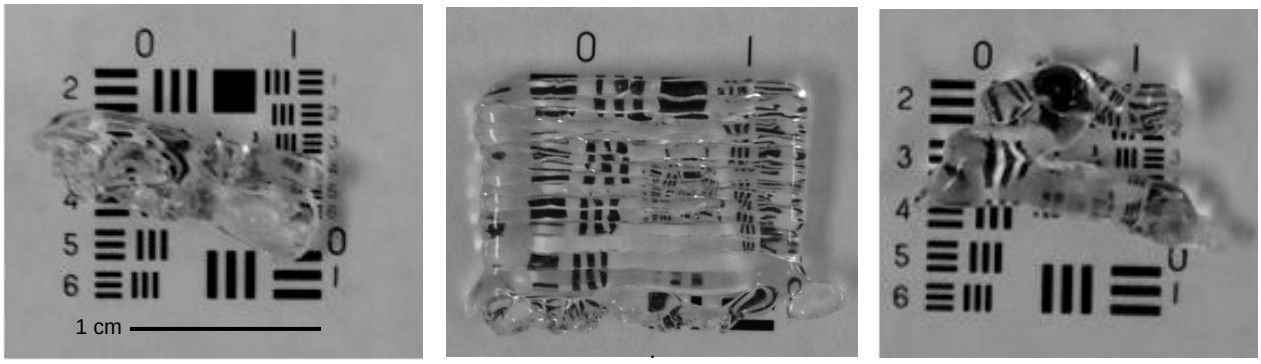

Fig. 2. (a) A failed underfed wall (25 W) (b) A good wall (35 W) (c) A failed over melted wall (60 W)

Melt pool spectral results

As shown in Fig. 1(b), the melt pool constantly emits incandescent light during deposition. The spectrometer was used to measure this radiation melt pool. This spectrometer was calibrated with an OceanOptics LS-1-CA 2800 K light source. As the objective of this study is to investigate the effects that different laser powers have on the transparency of printed fused quartz, the radiation spectrum data was collected when the laser beam was at the center of the path of travel on the fifth deposited layer. This was done to mitigate the effects of the substrate, and the edges of the walls and provide a correlation between emitted light and the temperature of the melt pool. The spectra is plotted in Fig. 3. As the emissivity of fused quartz has been shown to vary in respect to wavelength [21], the shape of radiation spectrum of fused quartz is significantly different with blackbody. For laser powers between 20 and 40 W, the radiation peak shifts towards shorter wavelengths as the laser power increases, according to Wein's displacement law. This trend is not observed for higher laser powers. Their spectral peak is invariant at λ=740 nm and the melt pool begins to release fumes. This suggests that the vaporization of the fused quartz stabilizes the temperature of the melt pool. The increase in intensity is due to the spectrometer interrogation area being up to three times larger than the melt

pool in normal operation. At high laser powers the melt pool is enlarged which is reflected in the recorded intensity. These spectrometer results are consistent with the experimental results found in Yang et. al. [22].

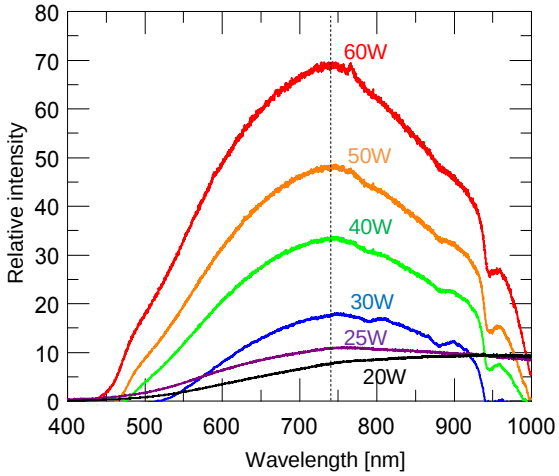

Fig. 3. Radiation spectra of fused quartz melt pools for in different laser powers

Optical results

The experimental refractive indices were measured after the fused quartz walls were polished with a 1 μm grit lap disk. This was done to separate the effects of surface refraction from the material transmittance. Polishing reduces refractive effects but introduces surface scatter. An ellipsometer (J.A. Woollam M-VASE) was used to measure the experimental refractive indices, and the results are plotted in Fig. 4. These measurements were consistent between the quartz walls printed at different powers. There are some differences between the measured indices of refraction and the published indices of refraction [23], mainly at low frequencies. This is most likely due to the Raleigh scattering of light from the polished surface finish.

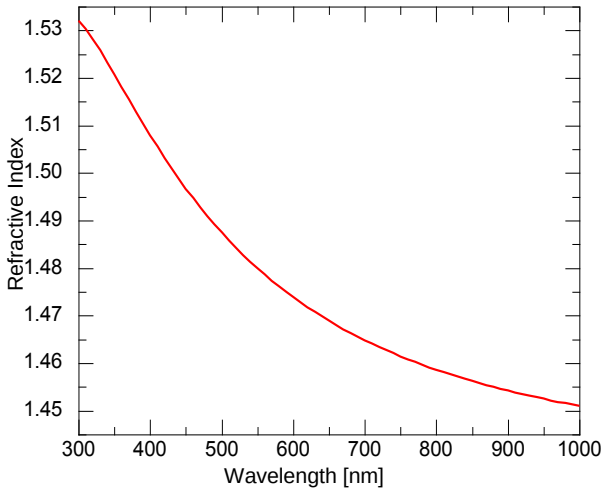

Fig. 4. Refractive index of fabricated fused quartz after polishing.

Even a perfectly polished flat quartz lens is not fully transmissive. There is some power loss due to Fresnel reflection, the Fresnel reflection at normal incidence is given by $R = [(1-n)/(1+n)]^2$ [24]. In the absence of absorptance the transmittance is equal to $(1\text{-}R)^2$. The actual transmittance was measured using an OceanOptics USB-4000 spectrometer. The fused quartz samples were placed at the focal point of the second lens so that the light scattered by the samples could be collected by the spectrometer. The transmittance is measured by normalizing the transmitted spectrum through the samples without the samples. In the experiment the sample was illuminated with a solid angle 0.7, and collected by the spectrometer with a solid angle 1.32. This permits some of the light scattered by imperfections in the polishing process as seen by to be collected. Figure 5 shows the transmittance of printed walls in different wavelengths. This result shows that the transmittance is not dependent on the laser power used to print it.

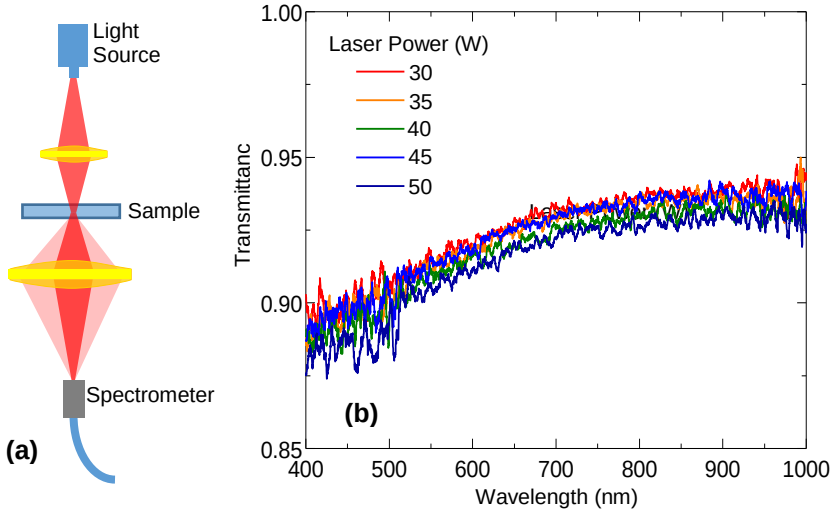

Fig. 5. (a) Transmittance measurement setup (b) Relative glass wall transmittance in visible spectrum range.

After accounting for reflection, the fused quartz is transparent within the measurement accuracy of the experiment at NIR wavelengths. The reduced transmission at shorter wavelengths may be due to Rayleigh scatter off of polishing defects. Another concern for printed optics is index homogeneity: making sure the index of refraction does not vary across the printed part for uniform material deposition. Even small variances in index of refraction may significantly degrade the optical performance of a system. To evaluate the index homogeneity, samples were inserted into the optical path of a simple microscope which was used to image a test pattern. This allowed the effects of adding the quartz to be quantified with the Modulation Transfer Function (MTF). MTF is a measure of the transfer of modulation (or contrast) from the subject to an image. In this study, the USAF 1951 was used as a test pattern. This pattern can be seen in Fig. 6(b). As the spatial resolution of the optical system decreases the modulation depth of the image, M, also decreases and the image becomes blurry. The parameter M is defined as [26]

$$M = \frac{A_{max} - A_{min}}{A_{max} + A_{min}} \tag{1}$$

where A_{max} is the maximum intensity and A_{min} is the minimum intensity in the lines pattern. Spatial frequency is measured in lines per mm (mm^{-1}). In order measure the transfer of modulation, the test samples were separated from the object by 30 mm when each sample was photographed. This experimental setup can be seen in Fig. 6. The MTF of each of the experimental samples, and that of a microscope slide, were calculated using the line patterns of the 4th group of the USAF 1951 test pattern. The 4th pattern was chosen as its image, as produced by the optical system, contains lines that range from clear to blurry. The MTF results show that the spatial resolution of quartz walls is comparable to that of the microscope slide, and the laser power does not influence the resolution of the walls.

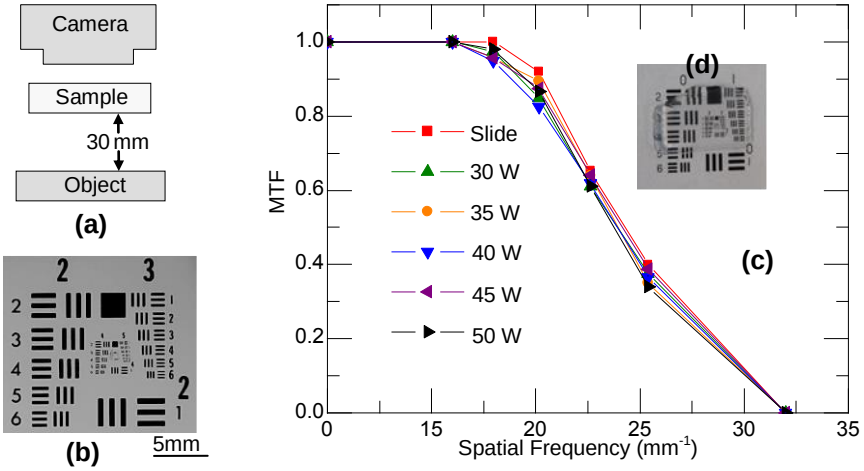

Fig. 6. (a) Method for image measurements (b) an example of the images being analyzed (c) MTF results for all samples with inset showing photograph of entire test pattern.

For every optical system, there is an image too small for it to render. This limit is called cutoff spatial frequency. At this frequency $M = 0$, that is, the image is completely blurry and there is no distinction between shapes [26]. The cut off spatial frequency for the optical system used in the MTF experiment was calculated to be $\xi_{cutoff} = 1/(\lambda\ F/\#) = 181\ mm^{-1}$, where λ is the wavelength of light which is assumed to be 550 nm, $F/\#$ is the unitless f number of the camera, 10.

The spatial frequency of images that can be resolved using the experimental set up is much lower than ξ_{cutoff}. This is because the pixel length in the image is only 11 μm, the same magnitude of the line width that is being measured (17.54 μm), the pattern itself has a spatial frequency of 28.51 mm^{-1}. This implies that the limiting factor of measuring the clarity of the experimental quartz pieces lies not with the quartz, nor the cutoff frequency, or even the diffraction limit, but with the resolution of the camera that was used to capture the image.

Thermal Analysis

Glass enters the melt pool as a filament and exits as a printed line as seen in Fig. 7. The density of glass is not strongly dependent on temperature and the mass balance can be expressed as:

$$\dot{m}_{in} = \frac{\pi}{4} D_f^2 \cdot f = \dot{m}_{out} = A_c \cdot v \tag{2}$$

where D_f is the diameter the filament and A_c is the cross sectional area of the printed track.

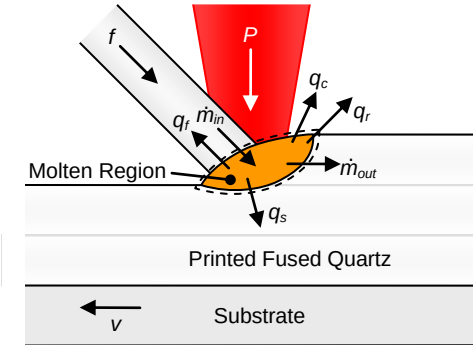

Fig. 7. Mass and energy balance surrounding melt pool.

At steady state the change in energy around the molten region is zero and is expressed as,

$$\Delta E = P - \left(\dot{m}\Delta h + q_s + q_f + q_c + q_r\right) = 0 \tag{3}$$

where P is the laser power, Δh is the specific enthalpy increase of the glass from inlet to outlet, q_s is the heat lost to the substrate, q_f is the heat transferred to the filament, and q_r and q_c represent the heat exchanged with the surroundings via radiation and convection, respectively. The heat transfer from the melt pool to the glass wall is a complex process with temperature dependent thermal properties. The following assumptions are made to significantly simplify the heat transfer analysis: 1) the temperature is uniform in the molten region; 2) the shape of the molten region is constant; 3) the convection coefficient is taken to be 10 W/m^2·K, and is temperature independent; and 4) the filament acts as an extended surface subject to convection and radiation, but advection is neglected.

Fused quartz is an amorphous material and transitions gradually from the solid to liquid phases. Unlike crystalline materials, there is no specific melting point or discrete enthalpy of fusion, so its temperature continues to rise as the viscosity decreases. Glass enters the control volume as a solid filament at room temperature, T_i, is heated by the laser until it leaves the control volume at the temperature of the melt, T_m, and begins to cool.

The heat transfer from the melt pool to the air includes convection (q_c) and radiation (q_r). For a hemispherical molten region of diameter, D_m, these are given, respectively, by

$$q_c = h\left(\frac{\pi}{4}D_m^2\right)\left(T_m - T_\infty\right) \tag{4}$$

and

$$q_r = \varepsilon\sigma\left(\frac{\pi}{4}D_m^2\right)\left(T_m^4 - T_\infty^4\right) \tag{5}$$

where h is the heat convection coefficient, T_∞ is the ambient temperature which is assumed to be the same as the surroundings, ε is the emissivity of glass, and σ is Stefan-Boltzmann constant.

The heat conduction from the laser heated spot through the substrate (q_s) was calculated using a Finite Volume Method (FVM) model in ANSYS FLUENT (a commercial thermo-fluid analysis package). The objective of the simulation is to relate the laser power to a representative temperature in the molten region. In the simulation, a laser beam was scanned along the center of an infinitely long rectangular wall. The simulation is allowed to progress until the temperature distribution is invariant with respect to distance. Practically, this involved scanning the laser for distances ranging from 40 to 60 mm, for a scan speed 0.5 mm/s, and for laser powers ranging from 20 W to 60 W. The relationship between T_m and q_s is

$$q_s = \begin{cases} 4\times10^{-5}T_m{}^2 - 0.216T_m + 264.08 & T \le 2827 \\ 0.4898T - 1344.3\,W & T > 2827 \end{cases} \tag{6}$$

where the temperature T is expressed in °C.

Since the diameter of the filament is small compared to its length, the heat conduction along the filament is assumed to be 1D, with a temperature only dependent the length direction (i.e., the direction in which it is fed). The temperature of the end connected with the melt pool is the average temperature of melt pool, and the temperature on the other end is the ambient temperature. The heat conducted into the filament is the sum of the heat convection and radiation from the filament to the air and the heat transferred by advection. A second order ODE is obtained by truncating the Taylor expansion of q_f

$$-\frac{d}{dx}\left(k\frac{dT_f}{dx}\right)\left(\frac{\pi D^2}{4}\right) - h_c\pi D\left(T_f - T_\infty\right) - \varepsilon\sigma\pi D\left(T_f{}^4 - T_\infty^4\right) - \rho A_c fc_p\frac{dT_f}{dx} = 0 \tag{7}$$

where D is the filament diameter, T_f is the temperature inside the filament, ρ is the density of glass. The boundary conditions are: $T = T_m$, $x = 0$; $T = T_\infty$, $x = \infty$. When T_m is known, the temperature distribution inside the filament is obtained by solving (7) numerically. The heat transferred into the filament is calculated from the temperature gradient ($q_f = k\,dT/dx|_{x=0}$) at the end of filament that is in the melt pool. Evaluating Eq. (7) using a finite difference approach shows that the heat transferred (q_f) into the filament also varies as a nearly linear function of the temperature of the molten region. For temperatures in excess of 1000°C and below the vaporization temperature and a 1 mm diameter filament, this can be approximated as

$$q_f = \left(2.600\times10^{-3}\,\mathrm{W/K}\right)T_m - 0.7771\,\mathrm{W} \tag{8}$$

The temperature of the molten region can be estimated by solving Eq. (3). The temperature of the molten region is plotted as a function of the laser power in Fig. 8. The melt pool temperature increases with the laser power linearly until it reaches 2827°C. Then it keeps nearly constant at 2827°C due to the vaporization of the fused quartz. This result is in consistent with the spectrometer result, which shows that the temperature does not vary in the laser power range of 40 to 60 W due to the remelting of the previous layers and the vaporization of the fused quartz.

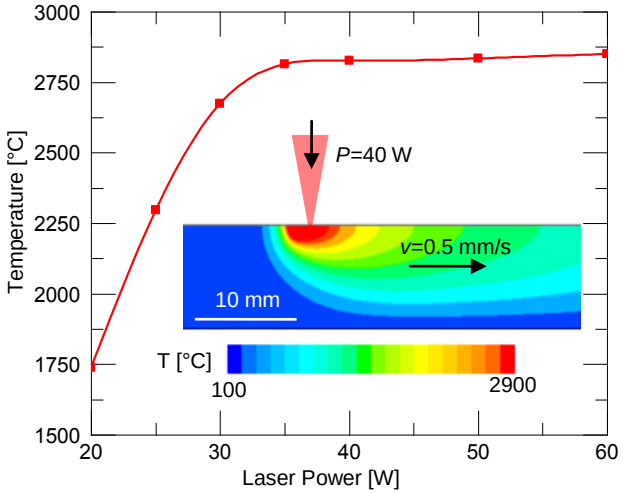

Fig. 8. Estimated molten region temperature using energy balance model for infinitely long wall.

Summary and Conclusions

This paper demonstrates the deposition of fused quartz parts using a filament fed additive manufacturing process. Good quartz walls can be made using the filament fed process with laser powers between 30 W and 50 W. Optical testing shows that the optical characteristics of these samples (index of refraction, transmittance, and index homogeneity) is independent of the laser power. This result is supported by low-order temperature modeling of the process which suggests that the temperature over this power range is determined by the vaporization point of quartz. Compared to soda-lime glass, fused quartz has several advantages for AM, including minimal reboil and spatial index variation, as well as high index homogeneity. Some of these phenomena can be explained by the low order model included in this paper. Future work will incorporate a precision motion system into the experimental set up. This will allow the creation of a process parameter map for the AM of quartz, as well as other materials like borosilicate glass and alumina.

References

[1] Pereira, T., Rusinkiewicz, S., and Matusik, W., 2014, "Computational Light Routing: 3D Printed Optical Fibers for Sensing and Display," ACM Transactions on Graphics (TOG), 33(3), p. 24.

[2] Willis, K., Brockmeyer, E., Hudson, S., and Poupyrev, I., 2012, "Printed optics: 3d printing of embedded optical elements for interactive devices," Proceedings of the 25th annual ACM symposium on User interface software and technology, ACM, Cambridge, MA, Oct. 7-10, pp. 589-598.

[3] Brockmeyer, E., Poupyrev, I., and Hudson, S., 2013, "PAPILLON: designing curved display surfaces with printed optics," Proceedings of the 26th annual ACM symposium on User interface software and technology, ACM, St. Andrews, Scotland, United Kingdom, Oct. 8-11, pp. 457-462.

[4] Urness, A. C., Moore, E. D., Kamysiak, K. K., Cole, M. C., and McLeod, R. R., 2013, "Liquid deposition photolithography for submicrometer resolution three-dimensional index structuring with large throughput," Light: Science & Applications, 2(3), p. e56.

[5] Niino, T., and Yamada, H., 2009, "Fabrication of Transparent Parts by Laser Sintering Process:-Transparentization of laser sintered plastic parts by infiltrating thermosetting epoxy with tuned refractive index," Journal of the Japan Society for Precision Engineering, 75(12), pp. 1454-1458.

[6] Marder, S. R., Brédas, J.-L., and Perry, J. W., 2007, "Materials for multiphoton 3D microfabrication," Mrs Bulletin, 32(07), pp. 561-565.

[7] Blessing, K., 2014, "Print head, upgrade kit for a conventional inkjet printer, inkjet printer and method for printing optical structures," U.S. Patent No. 8,840,235. (23 September 2014).

[8] Weber, M. J., 2002, Handbook of optical materials, CRC press, Boca Raton, FL.

[9] Khmyrov, R., Grigoriev, S., Okunkova, A., and Gusarov, A., 2014, "On the possibility of selective laser melting of quartz glass," Physics Procedia, 56, pp. 345-356.

[10] Klocke, F., McClung, A., and Ader, C., 2004, “Direct Laser Sintering of Borosilicate Glass,” Solid Freeform Fabrication Symposium Proceedings, Austin, TX, Aug. 3–5, pp. 214–219.

[11] Fateri, M., and Gebhardt, A., 2015, "Selective Laser Melting of Soda‐Lime Glass Powder," International Journal of Applied Ceramic Technology, 12(1), pp. 53-61.

[12] Luo, J., Pan, H., and Kinzel, E. C., 2014, "Additive Manufacturing of Glass," Journal of Manufacturing Science and Engineering, 136(6), p. 061024.

[13] Fu, Q., Saiz, E., and Tomsia, A. P., 2011, "Bioinspired strong and highly porous glass scaffolds," Advanced functional materials, 21(6), pp. 1058-1063.

[14] Klein, S., Simske, S., Adams, G., Parraman, C., Walters, P., Huson, D., and Hoskins, S., 2012, "3D Printing of Transparent Glass," Proc. NIP & Digital Fabrication Conference, Society for Imaging Science and Technology, Quebec City, Canada, Sep. 9-13, pp. 336-337.

[15] Marchelli, G., Prabhakar, R., Storti, D., and Ganter, M., 2011, "The guide to glass 3D printing: developments, methods, diagnostics and results," Rapid Prototyping Journal, 17(3), pp. 187-194.

[16] Mok, S. H., Bi, G., Folkes, J., Pashby, I., and Segal, J., 2008, "Deposition of Ti–6Al–4V using a high power diode laser and wire, Part II: Investigation on the mechanical properties," Surface and Coatings Technology, 202(19), pp. 4613-4619.

[17] Weber, M. J., 2002, Handbook of optical materials, CRC press, Boca Raton, FL.

[18] Kitamura, R., Pilon, L., and Jonasz, M., 2007, "Optical constants of silica glass from extreme ultraviolet to far infrared at near room temperature," Applied optics, 46(33), pp. 8118-8133.

[19] Syed, W. U. H., and Li, L., 2005, "Effects of wire feeding direction and location in multiple layer diode laser direct metal deposition," Applied Surface Science, 248(1-4), pp. 518-524.

[20] Mok, S. H., Bi, G., Folkes, J., and Pashby, I., 2008, "Deposition of Ti–6Al–4V using a high power diode laser and wire, Part I: Investigation on the process characteristics," Surface and Coatings Technology, 202(16), pp. 3933-3939.

[21] Pettersson, M., and Stenström, S., 2000, "Modelling of an electric IR heater at transient and steady state conditions: Part I: model and validation," International journal of heat and mass transfer, 43(7), pp. 1209-1222.

[22] Yang, S. T., Matthews, M. J., Elhadj, S., Draggoo, V. G., and Bisson, S. E., 2009, "Thermal transport in CO2 laser irradiated fused silica: in situ measurements and analysis," J. Appl. Phys, 106(10), p. 103106.

[23] I. H. Malitson, 1965, Interspecimen Comparison of the Refractive Index of Fused Silica, J. Opt. Soc. Am. 55, 1205-1208

[24] Born, M., and Wolf, E., 1999, Principles of optics: electromagnetic theory of propagation, interference and diffraction of light, CUP Archive, Cambridge, UK.

[25] Bohren, C. F., and Huffman, D. R., 2008, Absorption and scattering of light by small particles, John Wiley & Sons.

[26] Boreman, G. D., 2001, Modulation transfer function in optical and electro-optical systems.